



Regular Article

Multi-zinc oxide-cores@uni-barium sulfate-shell with improved photo-, thermal-, and ambient-stability: Non-equilibrium sorption fabrication and light-emitting diodes application



Ya-Chuan Liang ^a, Kai-Kai Liu ^{b,c,*}, Xue-Ying Wu ^a, Xian-Li Lu ^a, Ying-Jie Lu ^a, Qi Zhao ^{a,*}, Chong-Xin Shan ^{a,c,*}

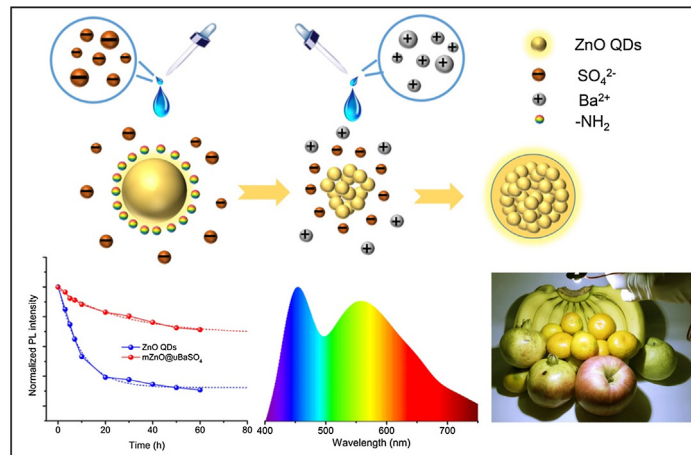
^a School of Physics and Engineering, Zhengzhou University, Zhengzhou 450001, China

^b State Key Laboratory of Luminescence and Applications, Changchun Institute of Optics, Fine Mechanics and Physics, Chinese Academy of Sciences, No. 3888 Dongnanhu Road, Changchun 130033, China

^c University of the Chinese Academy of Sciences, Beijing 100049, China

GRAPHICAL ABSTRACT

Multi-zinc oxide-cores@uni-barium sulfate-shell nanocomposite has been prepared via non-equilibrium sorption process, and the nanocomposite shows improved stability in photo, thermal and ambient aspects. WLED has been fabricated by using the nanocomposite phosphors as down-conversion layer. Thanks to the abundance and eco-friendly property of ZnO, the result reported in this paper may open a promising avenue for healthy WLEDs.



ARTICLE INFO

Article history:

Received 12 April 2018

Revised 15 May 2018

Accepted 28 May 2018

Available online 29 May 2018

Keywords:

mZnO@uBaSO₄ nanocomposite

ABSTRACT

ZnO as an eco-friendly material shows bright luminescence under UV illumination when it is tailored into nanoscale size, which makes it a promising luminescent nanomaterial. However, the poor stability of ZnO hinders its applications drastically. In this work, multi-ZnO-cores@uni-BaSO₄-shell (mZnO@uBaSO₄) nanocomposite has been prepared through a non-equilibrium sorption process employing ZnO QDs as the "seeds" and BaSO₄ as the "valve". The mZnO@uBaSO₄ nanocomposite shows improved photo-, thermal- and ambient-stability compare with bare ZnO QDs. The fluorescence efficiency of the mZnO@uBaSO₄ nanocomposite decreases little even after 60 h of UV irradiation compare with ZnO QDs. The mZnO@uBaSO₄ nanocomposite shows bright luminescence with little decrease even the

* Corresponding authors at: State Key Laboratory of Luminescence and Applications, Changchun Institute of Optics, Fine Mechanics and Physics, Chinese Academy of Sciences, No. 3888 Dongnanhu Road, Changchun 130033, China (K.-K. Liu); University of the Chinese Academy of Sciences, Beijing 100049, China (C.-X. Shan).

E-mail addresses: liukaikai@ciomp.ac.cn (K.-K. Liu), zhaoqi@126.com (Q. Zhao), cxshan@zzu.edu.cn (C.-X. Shan).

Phosphors
Light-emitting diodes

ambient temperature up to 160 °C and the nanocomposite shows strong resistance to harsh environment. By coating the mZnO@uBaSO₄ nanocomposite and commercial phosphors onto UV-chip, light-emitting diode (LED) with correlated color temperature, Commission Internationale de L'Eclairage coordinate, color rendering index and luminous efficiency of 6109 K, (0.32, 0.33), 85 and 47.33 lm/W have been realized, and this will make a great step towards eco-friendly UV-pumped LEDs.

© 2018 Elsevier Inc. All rights reserved.

1. Introduction

In recent years, UV-pumped white light-emitting diodes (WLEDs) have attracted much attention due to their merits of less blue emission, higher luminous efficiency, broader spectrum, and higher color rendering index (CRI) compare to blue-light-pumped WLEDs [1–6]. To date, commercial WLEDs are usually realized by coating yellow phosphors onto blue light chips, and the phosphors emit yellow light under blue light illumination, and white luminescence can be obtained when yellow and blue light are mixed [7–11]. However, the excess blue emission, the lower luminous efficiency and CRI of blue-light-pumped WLEDs drive people to go after efficient and healthy WLEDs [12–15]. No matter in fabricating UV-pumped or blue light-pumped WLEDs, phosphors as down-conversion layer play a key role in determining the performance of WLEDs [16–20]. Conventional phosphors are rare-earth-based and Cd ions based quantum dot (QD) phosphors [21–27]. However, there are still some limitations and disadvantages to be taken seriously. Firstly, rare earths are non-renewable resources, and the reservation is limited. Secondly, the mining and purifying of rare earths often involves complex operations, which result in environmental pollution. Thirdly, high-performance QDs usually involve Cd ions, leading to toxicity concerns [21,28]. As an eco-friendly material, ZnO will show bright luminescence when it is tailored into nanoscale size [29]. Benefit from its eco-friendly character and high quantum yields (QYs) [27,30,31], ZnO QDs have been widely used in many fields, such as bioimaging [32–34], drug delivery [35–38], labeling [39–41], and photovoltaic devices [41–44], etc. It had been proved that ZnO QDs as nano-emitters are suitable for fabrication electric-pumped LED. For example, Son *et al.* reported a novel and simple chemical method for synthesizing emissive ZnO-graphene QDs, and WLEDs with brightness of 798 cd m⁻² based on the QDs had been demonstrated [45]. Chen *et al.* reported all solution-processed white QD-LED by using hybrid ZnO@TiO₂ as blue emitters and electron injection layer. The maximum luminance and power efficiency of the white QD-LED are 730 cd m⁻² and 1.7 lm W⁻¹, respectively [46]. However, it is quite challenging and difficult to exactly stack various layers together for solution-processed WLEDs. Besides, the luminous efficiency and luminous intensity of the LEDs are still below expectation, and this will limit their practical application. UV-chips as pumped light are easy to fabricate high-performance LEDs, which have attracted increasing attention. In our previous work, we developed a way to large-scale synthesis of ZnO QDs with high QYs, and yellow LEDs have been fabricated successfully by coating the ZnO QD phosphors onto UV chips, indicating ZnO QDs may have great potential in UV-pumped WLEDs [27]. Nevertheless, the poor stability of ZnO QDs in photo-, thermal- and ambient-aspects (especially photo-stability) limits their application in UV-pumped WLEDs. Therefore, it is interesting but still a challenge to develop ZnO based phosphors with high photo-, thermal- and ambient-stability to reduce or substitute the usage of rare-earth-based and Cd ions based phosphors, and this will make a great contribution to eco-friendly UV-pumped WLEDs.

BaSO₄ was well known for its high stability. Therefore, BaSO₄ was expected to provide a stable shell for ZnO QDs, which can

greatly improve the stability of ZnO QDs. In this work, multi-ZnO-cores@uni-BaSO₄-shell (mZnO@uBaSO₄) nanocomposite has been prepared via a non-equilibrium sorption process, and the nanocomposite shows greatly improved photo-, thermal- and ambient-stability compared with bare ZnO QDs. In this process, ZnO QDs with positive charges maintain electrostatic equilibrium before addition of SO₄²⁻ ions, while the electrostatic equilibrium is broken when SO₄²⁻ ions are added and the ZnO QDs aggregate into multi-ZnO-cores luminescent centers. Then by adding Ba²⁺ ions into the solution, BaSO₄ shells grow around the surface of luminescent centers, which form mZnO@uBaSO₄ nanocomposite. In this structure, BaSO₄ shell acts as a protective layer that provides a protection for the ZnO luminescent center. The BaSO₄ matrix neither competes for absorbing excitation light nor absorbs the emissions of ZnO QDs, which is favor of keeping quantum yield while improving stability. The resultant mZnO@uBaSO₄ nanocomposite possesses obvious comparative advantages: Firstly, the fluorescence efficiency of the mZnO@uBaSO₄ nanocomposite decrease little even after sixty hours of UV irradiation compare with ZnO QDs. Secondly, the mZnO@uBaSO₄ nanocomposite shows bright luminescence with little decrease even the ambient temperature up to 160 °C, indicating it can be used as heat-resist phosphors. Thirdly, the nanocomposite shows strong resistance to acid, alkali and organic, which promising their potential applications in harsh environment. White light-emitting diodes (WLEDs) with correlated color temperature (CCT), Commission International de L'Eclairage (CIE) coordinate and color rendering index (CRI) of 6109 K, (0.32, 0.33) and 85 have been realized by employing the mZnO@uBaSO₄ and commercial phosphors as luminescent phosphors.

2. Results and discussion

Water-soluble ZnO QDs are necessary for the preparation of mZnO@uBaSO₄ nanocomposite in view of the solubility of precursors BaCl₂ and NaSO₄. The ZnO QDs were prepared according to the method reported in our previous work [27]. The particle sizes of ZnO QDs are about 5 nm in this work and they will emit yellow illumination under UV radiation (Fig. S1, Supporting Information). In addition, the water-soluble ZnO QDs possess positive charges due to the existence of amino (Fig. S2, Supporting Information), which pave the way to prepare mZnO@uBaSO₄. The formation process of the mZnO@uBaSO₄ nanocomposite was illustrated in Fig. 1 (a). Firstly, the ZnO QDs are modified by APTES which can endow the QDs good water-soluble characters (Fig. 1b1). On the other hand, ZnO QDs with silica layer can avoid quenching when they aggregate into cores. For preparation mZnO@uBaSO₄, ZnO QDs are first premixed with Na₂SO₄ aqueous solution, SO₄²⁻ ions are attracted on the surface of the ZnO QDs due to the electrostatic adsorption effect. The zeta potential of the mixed aqueous solution changes from +37.4 mV to -0.14 mV (Fig. S3, Supporting Information), indicating that SO₄²⁻ ions have been attached onto the surface of the ZnO QDs. In this process, the electrostatic equilibrium of the ZnO QDs is broken when SO₄²⁻ ions are added and the ZnO QDs aggregate into multi-ZnO-cores luminescent centers following by

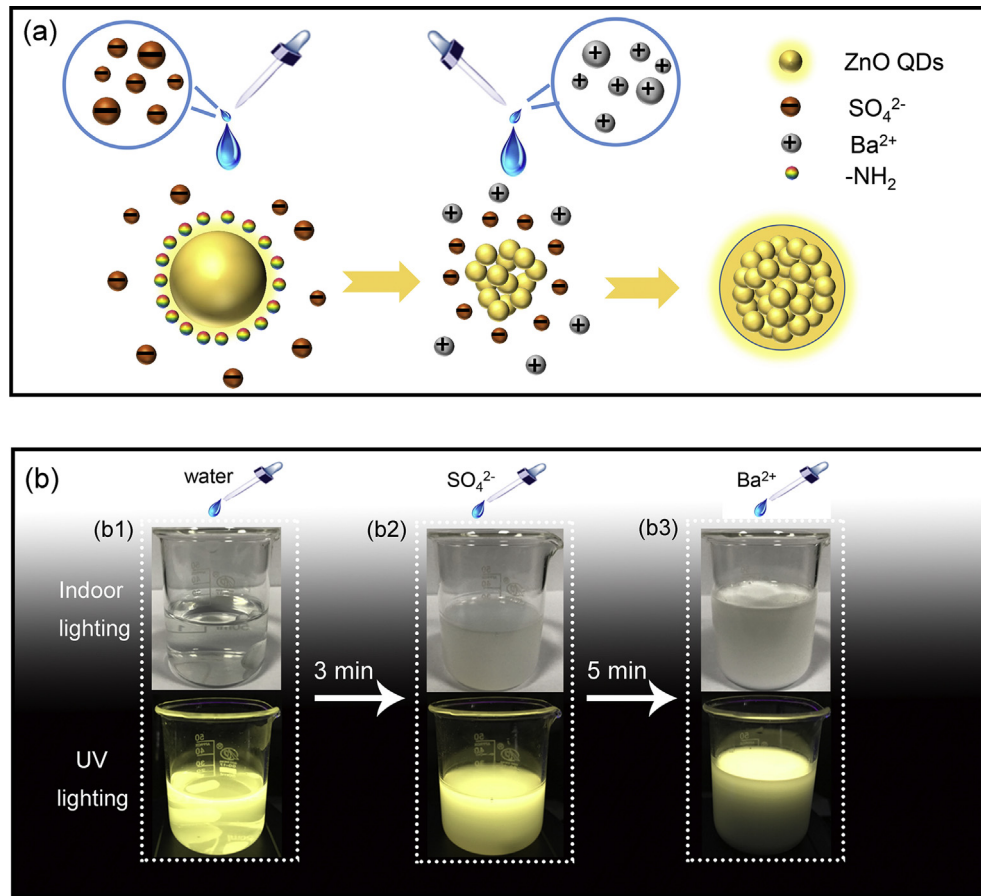


Fig. 1. Schematic illustration of the formation process of the mZnO@uBaSO₄.

the turbid of solution (Fig. 1b2). Finally, BaSO₄ shells grow around the surface of luminescent canters with the introduction of Ba²⁺ ions and the solution turns into milky white, indicating the mZnO@uBaSO₄ nanocomposite has been formed (Fig. 1b3). The strategy reported in this paper is related to surface charges of QDs, which is also suitable for those QDs with negative or positive charges.

Note that all the above processes are performed at room temperature, and over 21 g mZnO@uBaSO₄ powders can be synthesized in one synthesis process, as shown in Fig. 2(a), which lay a solid foundation for their future applications. The typical morphological and structural characterizations of the mZnO@uBaSO₄ have been analyzed by transmission electron microscope (TEM) and scanning electron microscope (SEM). The SEM image of the mZnO@uBaSO₄ shown in Fig. 2(b) reveals clearly that the as-prepared mZnO@uBaSO₄ nanocomposite consist of well-dispersed spherical shapes with diameter of 50–250 nm. The mean size of the mZnO@uBaSO₄ nanocomposite is 137.8 ± 2.9 nm and the size distribution is shown in the inset of Fig. 2(b). For comparison, bare BaSO₄ powders were also prepared by mixing BaCl₂ and Na₂SO₄ aqueous solution. The BaSO₄ precipitates have different diameters and irregular shapes (Fig. S4, Supporting Information). The difference in size and morphology are attributed to the presence of ZnO QDs, and the ZnO QDs act as cores in the formation of mZnO@uBaSO₄ nanocomposite process, leading to larger size of the nanocomposite. TEM image of the mZnO@uBaSO₄ nanocomposite confirms its spherical shape structure, and the ZnO QDs act as cores, and BaSO₄ as shells as shown in Fig. 2(c). The inset of Fig. 2(c) is the magnification image of an individual mZnO@uBaSO₄. The shadows in the spherical shape are the multi-ZnO-cores, indicating

that ZnO QDs have been uniformly coated with BaSO₄ shell. Fig. 2(d) shows the high-resolution TEM image of the mZnO@uBaSO₄ nanocomposite. Interplanar spacing with a distance of around 0.21 nm in the margin of the nanocomposite can be observed, which can be attributed to the BaSO₄ crystallites, while the interplanar spacing with a distance of around 0.26 nm corresponds to the inter-planar distances of the (0 0 1) plane of wurtzite ZnO. X-ray diffraction (XRD) patterns of the mZnO@uBaSO₄, ZnO QDs, and BaSO₄ have been investigated, as shown in Fig. 2(e). The broad peaks of ZnO QDs correspond well to hexagonal wurtzite structure (JCPDS 89-1397). The patterns of the mZnO@uBaSO₄ fit well to the structure of crystalline BaSO₄ powder. There are no characteristic diffraction peaks of ZnO QDs is visible because they are rather weak compared with those of crystalline BaSO₄. The element composition of the mZnO@uBaSO₄ characterized by EDS was indicated in Fig. 2(f), and Zn, O, Ba, S can be found in the sample, indicating the existence of ZnO QDs in the mZnO@uBaSO₄ nanocomposite. According to the EDS analysis, the fraction of Zn atoms in the mZnO@uBaSO₄ nanocomposite is about 20.29% and the corresponding atomic percentages of the mZnO@uBaSO₄ nanocomposite are shown in the inset of Fig. 2(f).

The excitation-emission matrix of the mZnO@uBaSO₄ nanocomposite powders is shown in Fig. 3(a). The emission range of the mZnO@uBaSO₄ nanocomposite powders is from 530 to 600 nm, and the corresponding optimal excitation range is from 340 to 370 nm, indicating the highest brightness emission of the mZnO@uBaSO₄ powders can be achieved under UV radiation and the powders can be used as UV-pumped down-conversion layer. To investigate the origins of the ZnO QDs, transient photoluminescence spectrum of the ZnO QDs has been measured and the

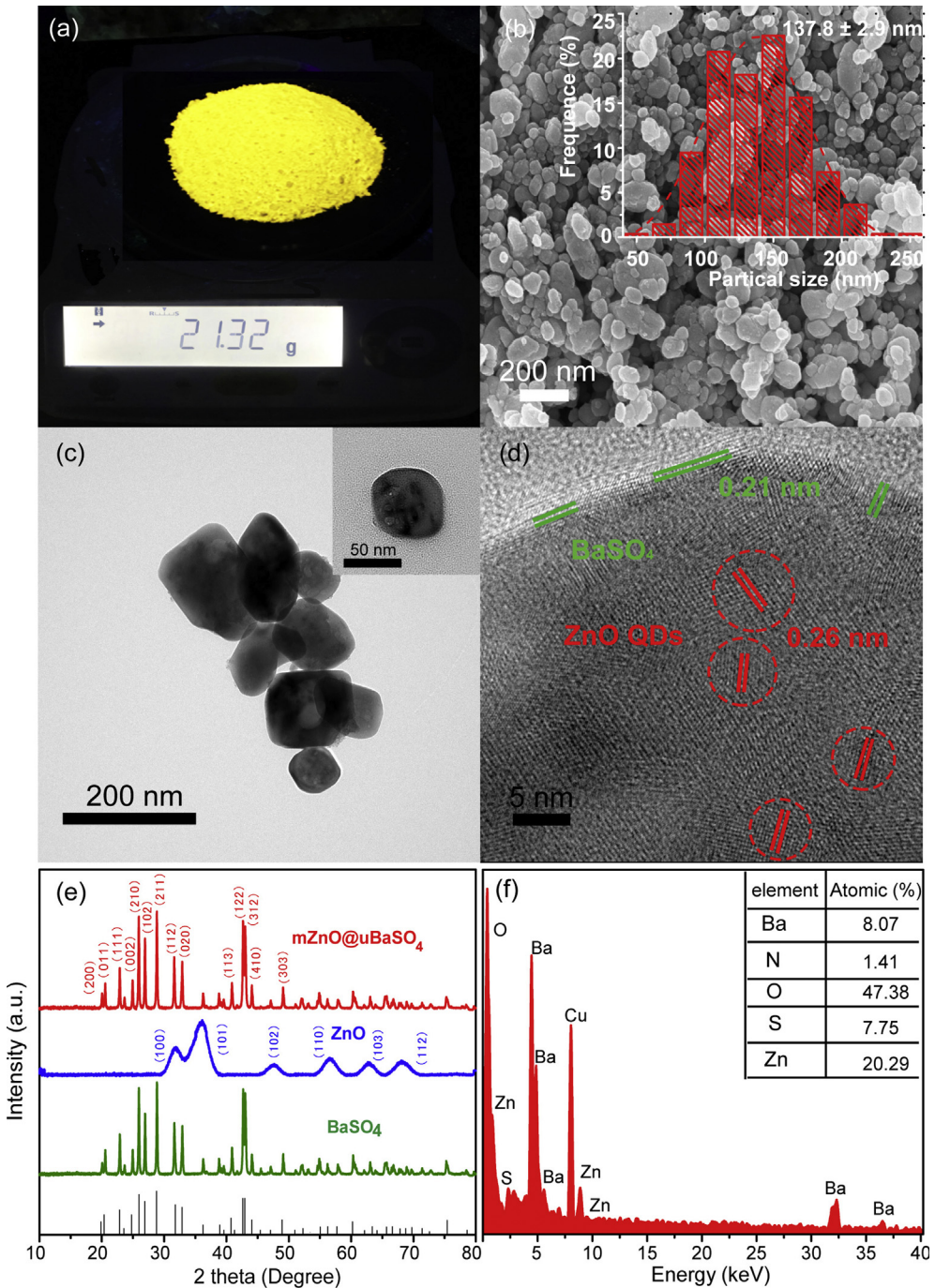


Fig. 2. (a) Image of the mZnO@uBaSO₄ nanocomposite powders. (b) SEM image of the mZnO@uBaSO₄ and the inset is the statistical size distribution of the mZnO@uBaSO₄ nanocomposite. (c) TEM image of the mZnO@uBaSO₄ and the inset shows the magnified image. (d) High resolution TEM image of the mZnO@uBaSO₄ nanocomposite. (e) XRD pattern of the mZnO@uBaSO₄, ZnO QDs and BaSO₄. (f) EDS pattern and element content of the mZnO@uBaSO₄.

corresponding results are recorded in Table S1 (Supporting Information). Here τ_1 may stem from the deep-level recombination inside the ZnO QDs; while τ_2 may stem from the oxygen vacancies which responsible for yellow emission of ZnO QDs. Fig. 3(b) shows the photoluminescence (PL) spectra of the ZnO QDs and mZnO@uBaSO₄ powders, and it can be seen that the mZnO@uBaSO₄ powders possess the same emission peak with ZnO QDs, which indicates that the BaSO₄ shell around the multi-ZnO-cores doesn't deteriorate the emission of the ZnO QDs. The mZnO@uBaSO₄ powders are white in color and show a strong yellow fluorescence under UV illumination (inset of Fig. 3b). BaSO₄ precipitate has been obtained by mixing BaCl₂ and Na₂SO₄ solu-

tion, and no fluorescence can be observed and the corresponding fluorescence spectra and photographs of bare BaSO₄ are shown in Fig. S5. Under the excitation of 365 nm line, the photoluminescence quantum yield (PLQY) of the mZnO@uBaSO₄ powders is 37.8%, slightly higher than that of ZnO QDs (35.8%). The increased PLQY is resulted from the less non-radiative transition centers compared with bare ZnO QDs [7], which can be further proved by their PL decay spectra, as indicated in Fig. 3(c). The transient spectra of the ZnO QDs can be well fitted employing two-order exponential expression, and the average lifetime τ_{ave} is calculated to be 80.59 ns. While for the mZnO@uBaSO₄, the lifetime is 219.50 ns and the corresponding results are recorded in Table S1

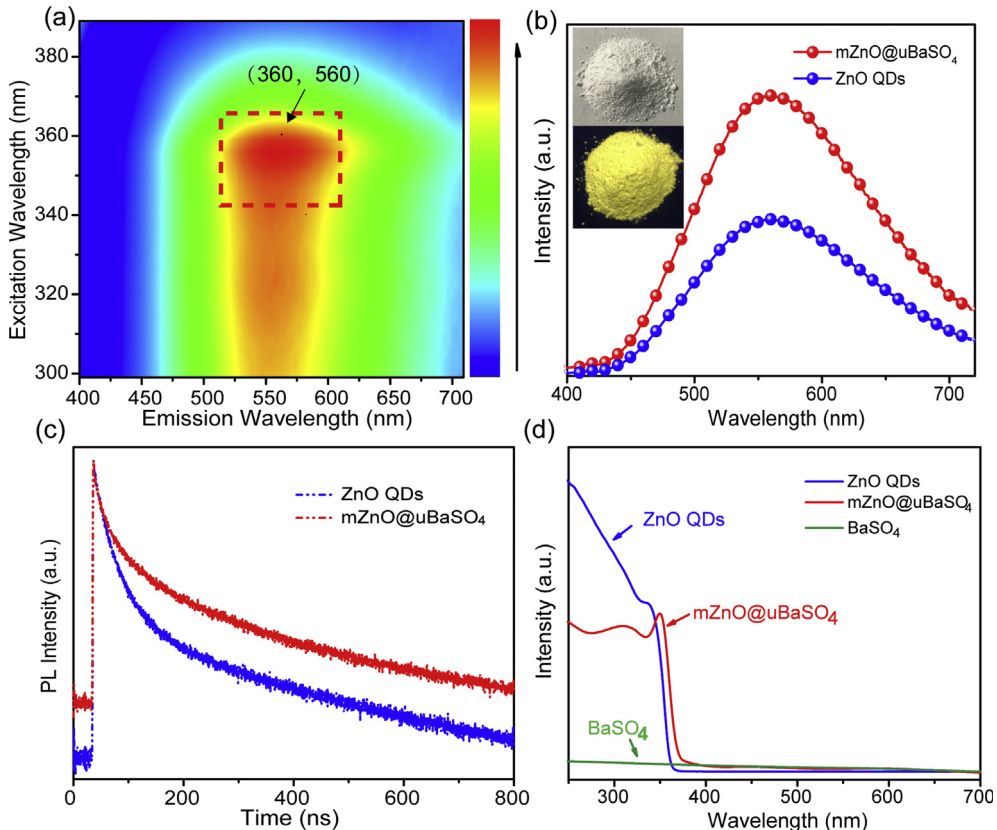


Fig. 3. (a) The excitation-emission matrix of the mZnO@uBaSO₄ nanocomposite powders. (b) Fluorescence spectra of the ZnO QDs and mZnO@uBaSO₄, and the inset shows the corresponding images of the mZnO@uBaSO₄ nanocomposite powders under indoor and UV lighting conditions. (c) Transient photoluminescence spectra of the ZnO QDs and mZnO@uBaSO₄. (d) Absorption spectrum of the ZnO QDs, mZnO@uBaSO₄ and BaSO₄.

(Supporting Information). From the PL decay curves, it can be seen that the luminescence lifetime of the mZnO@uBaSO₄ is longer than that of ZnO QDs, revealing that non-radiative centers decreases in the mZnO@uBaSO₄ nanocomposite. The reasons maybe that the non-radiative transition centers of the ZnO QDs are eliminated in the process of embedding and result in the increase of radiative transition rates during the non-equilibrium sorption process. The UV-Vis absorption spectra of the ZnO QDs, mZnO@uBaSO₄, and BaSO₄ are shown in Fig. 3(d). ZnO QDs and mZnO@uBaSO₄ show analogous maximum absorption peak at 360 nm, which can attribute to the near-band-edge absorption of ZnO. Note that BaSO₄ shows little absorption in the UV and visible region, indicating the emission from multi-ZnO-cores will not be absorbed by the BaSO₄. The above results show that BaSO₄ has almost no influence in absorption and emission band of ZnO QDs, leading to efficient photon emitting from the mZnO@uBaSO₄.

In our previous work, ZnO QDs will decompose when surrounding pH value is lower than 5.5, which means that the ZnO QDs are unstable [30]. To test the stability of the mZnO@uBaSO₄ nanocomposite, the ZnO QDs and mZnO@uBaSO₄ nanocomposite are placed in ethanol solution with pH value varies from 1 to 12, and the corresponding fluorescence images are shown in Fig. 4. Also, it is an effective way to verify whether the ZnO QDs are coated by BaSO₄ shell or not. The fluorescence of the ZnO QDs decreases greatly with the decreases of pH value, and it vanishes almost completely when the pH value of solution is smaller than 5, indicating the ZnO QDs dissolve in the acid solution completely (Fig. 4a). In addition, the fluorescence of the ZnO QDs will also decrease in alkaline environment, as shown in Fig. 4(a). The corresponding PL spectra are shown in Fig. S6(a). The dependence of the fluorescence intensity of ZnO QDs on the pH value of the solution is shown in Fig. 4(b), and the maximum fluorescence intensity occurs

when the pH value is 7. The above data indicate that the ZnO QDs are very sensitive to the surrounding pH values, and the fluorescence even vanishes when they are put in acidic conditions. Fig. 4(c) shows the fluorescence images of the mZnO@uBaSO₄ powders soaked in ethanol solution with pH values from 1 to 12 for 5 h. Compared to the ZnO QDs, the fluorescence intensity of the mZnO@uBaSO₄ powders changes little in acidic and alkaline environment, indicating the BaSO₄ shell encapsulates multi-ZnO-cores completely and can separate ZnO QDs with the outside environment effectively. The corresponding PL spectra are shown in Fig. S6(b) and the fluorescence intensity of the mZnO@uBaSO₄ versus surrounding pH value is shown in Fig. 4(d). Note that the fluorescence intensity of the mZnO@uBaSO₄ powders keeps almost unchanged in different pH value surroundings. The improved acidic and alkaline environment resistance of the mZnO@uBaSO₄ powders promises their application in harsh environment.

The stability of phosphors is a key issue that determines the performance of WLEDs, thus the stability of the mZnO@uBaSO₄ and bare ZnO QDs in photo, thermal and ambient aspects is accessed. The PL intensity of the mZnO@uBaSO₄ and ZnO QDs powders along with the UV illumination (0.15 mW/cm²) is shown in Fig. 5(a) and corresponding testing process is shown in Fig. S7. The scattered symbols are experimental data and the dot lines are the fitting results of the experimental data using the following single-order exponential decay formula:

$$y = y_0 + A_1 \exp(-x/t) \quad (1)$$

where y is the emission intensity, y_0 , A_1 are constants, and t is time. The PL intensity of the ZnO QD powders will decrease to about 30% of the initial intensity after 60 h of continuous radiation under UV illumination, while that of the mZnO@uBaSO₄ powders can maintain more than 70% after 60 h of UV illumination, as

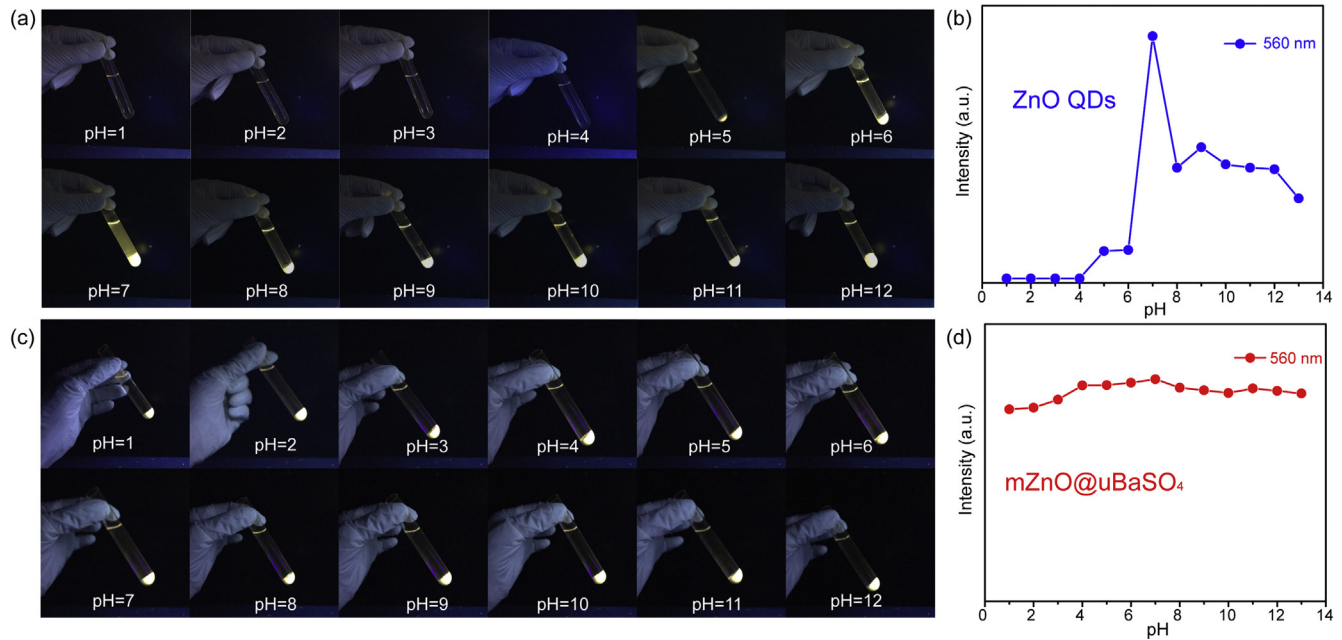


Fig. 4. (a) The fluorescence images of the ZnO QDs in solution with different pH values from 1 to 12. (b) The fluorescence intensity of the ZnO QDs powders in solution with different pH values from 1 to 12. (c) The fluorescence images of the mZnO@uBaSO₄ powders were soaked in solution with different pH values from 1 to 12 for 5 h. (d) The fluorescence intensity of the mZnO@uBaSO₄ powders in solution with different pH values from 1 to 12.

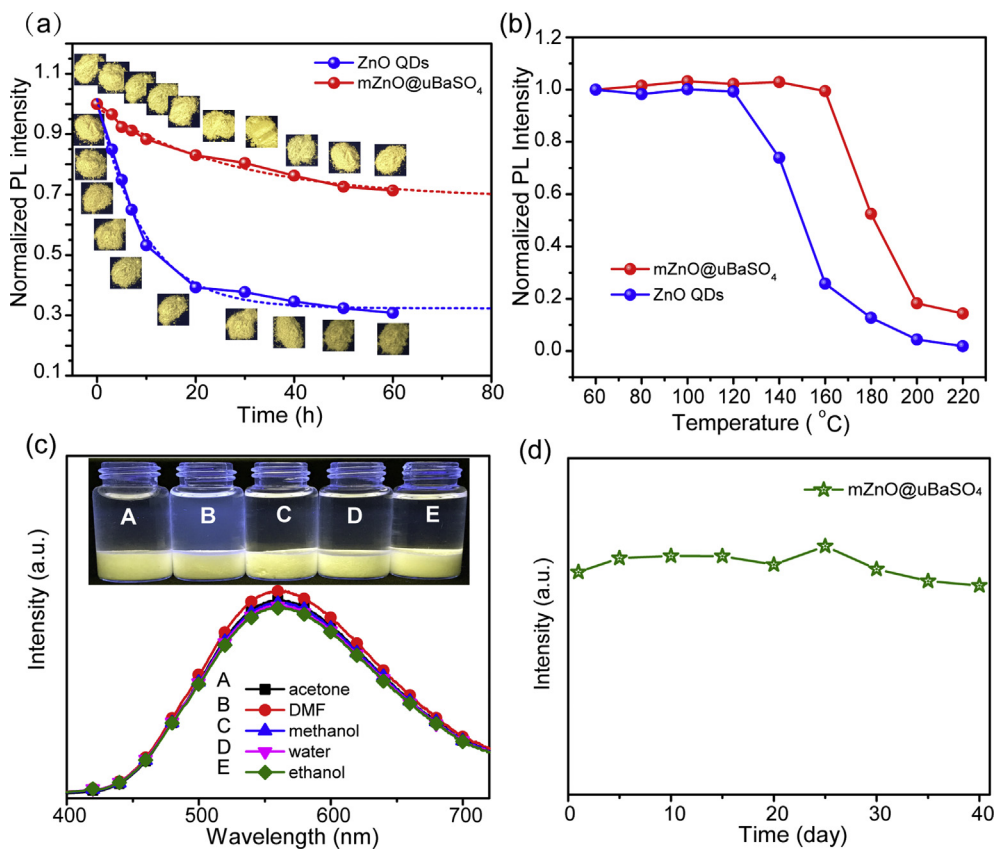


Fig. 5. (a) The photostability of the ZnO QDs and mZnO@uBaSO₄ powders. (b) The fluorescence intensity of the ZnO QDs and mZnO@uBaSO₄ powders after annealing. (c) The fluorescence spectra and image of the mZnO@uBaSO₄ powders sediment in acetone, dimethyl formamide, methanol, ethanol, and water. (d) The temporal stability of the mZnO@uBaSO₄ powders.

indicated in Fig. 5(a). The insets of the figure show the optical images of the mZnO@uBaSO₄ and ZnO QDs powders under UV illumination at different time intervals, and it is obvious that the emis-

sion of the ZnO QDs powders decreases significantly while that of the mZnO@uBaSO₄ powders decreases little in the investigated range, indicating that the mZnO@uBaSO₄ powders have better

photostability than bare ZnO. The improved photo-stability of the mZnO@uBaSO₄ powders ensures their PL stability under long time ultraviolet radiation when packaged it on UV chips.

Thermal stability is another important indicator for phosphors used in LEDs, thus the thermal stability of the ZnO QDs and mZnO@uBaSO₄ powders is analyzed. The samples were annealed in an oven with temperature from 60 to 220 °C for 30 min and the corresponding peak centered at 560 nm and PL intensity of the ZnO QDs and mZnO@uBaSO₄ powders after heat treatment are recorded, as shown in Fig. 5(b) and Fig. S8. As shown in Fig. 5(b), when the annealing temperature increases from 60 to 160 °C, the luminescence intensity of the mZnO@uBaSO₄ powders can maintain constant. While for bare ZnO QDs, the luminescence intensity begins to decreases when the annealing temperature is above 120 °C. The above results indicate that the thermal stability of the mZnO@uBaSO₄ powders is better than that of the bare ZnO QD powders. In addition, the mZnO@uBaSO₄ powders show stability to some common organic solvents such as acetone, dimethyl formamide, methanol, ethanol and water. The PL spectra of the mZnO@uBaSO₄ powders sediment in these organic solvents are shown in Fig. 5(c), and the corresponding images are shown in

the inset of Fig. 5(c). The PL spectra of the mZnO@uBaSO₄ powders reveal that the emission of the mZnO@uBaSO₄ powders is stable in the organic solvents and no emissions are observed in the supernatant solution (Fig. S9, Supporting Information), indicating the good ambient stability of the mZnO@uBaSO₄ powders, and the ambient-stability ensure that the mZnO@uBaSO₄ powders can maintain high luminous efficiency in the packaging process. The temporal stability of phosphors is also a key issue that determines the performance of WLEDs when they keep working for a long time, thus the temporal stability of the mZnO@uBaSO₄ powders is analyzed under ambient conditions. The corresponding PL spectra are shown in Fig. S10 and the peak centered at 560 nm is recorded in Fig. 5(d). The line shape and fluorescence intensity of powders keep almost unchanged within 40 days, indicating the good stability of the mZnO@uBaSO₄ powders synthesized in this route. Obviously, the improved photo-, thermal- and ambient-stability of the mZnO@uBaSO₄ powders compare to ZnO QDs ensures that the mZnO@uBaSO₄ powders can keep high performance when employed as phosphors in WLEDs. Another common inorganic material used for modifying QDs is SiO₂. For comparison, we attempt to embed ZnO QDs into SiO₂ matrix through Stober

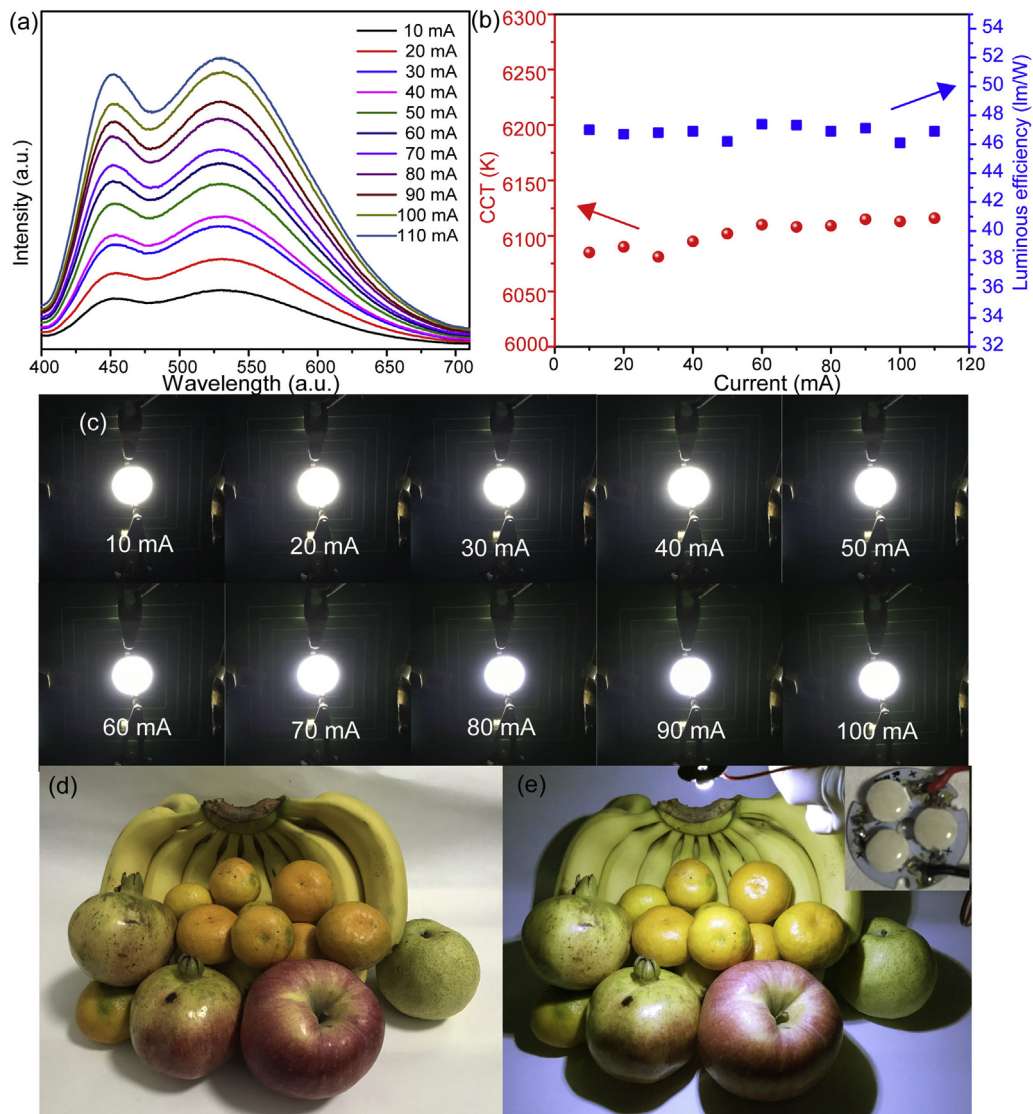


Fig. 6. (a) EL spectra of the UV chips coated with the mZnO@uBaSO₄ phosphors under different driven currents from 10 mA to 110 mA. (b) CCT and luminous efficiency of the fabricated LED under different driven currents. (c) Images of the WLED under different drive currents. (d) Images of some fruits under the illumination of sunlight and the WLEDs (e).

method and the stability of the ZnO@SiO₂ nanocomposite is analyzed. The ZnO@SiO₂ nanocomposite is placed in ethanol solution with pH value of 1, 2, 4, 7, 9, 12, and the corresponding fluorescence images are shown in Fig. S11. The fluorescence intensity of the ZnO@SiO₂ decreases greatly in the acid and alkaline solution indicating ZnO@SiO₂ nanocomposite is unstable in harsh environment. In addition, the fluorescence intensity of the ZnO@SiO₂ powders under continuous UV illumination is shown in Fig. S12. The fluorescence intensity of the ZnO@SiO₂ powders will decrease to about 50% of the initial intensity after 10 h of continuous UV radiation, while that of the mZnO@uBaSO₄ powders can maintain more than 70% after 60 h of under UV illumination reported in this paper. The possible reason is that above encapsulation strategies rely on physical adsorption and ZnO QDs cannot be packaged completely.

As discussed above, the mZnO@uBaSO₄ powders have improved photo-, thermal-, and ambient-stability compare to the bare ZnO QD powders. Based on the above advantages, UV-pumped LEDs have been fabricated by coating the mZnO@uBaSO₄ powders and commercial blue phosphors mixtures onto 365 nm UV-chips. The luminescence spectra of the LEDs can be adjusted by varying the mass ratios of these two phosphors, and the corresponding electroluminescence (EL) spectra of the LEDs are shown in Fig. S13(a). The spectra of the as-fabricated LEDs consist of two emission bands peaked at 450 nm and 560 nm, which can be assigned to the emission of commercial and mZnO@uBaSO₄ phosphors, respectively. The corresponding PL spectra of commercial phosphors are shown in Fig. S14. By adjusting the intensity ratio of the commercial and mZnO@uBaSO₄ phosphors (7:1(A), 4:1(B), 3:1(C), 2.2:1(D), 1.7:1 (E), 1.4:1(F), 1.1:1(G), 0.97:1(H), 0.67:1(I)), the correlated color temperature (CCT) of the LEDs can be tuned from 8858 K to 3770 K and the CIE color coordinates shift from (0.20, 0.14) to (0.42, 0.48), as shown in Fig. S13(b). It can be seen that the LEDs can be tuned from cool white to warm white. White LED with the CIE coordinate of (0.32, 0.33) can be realized, which is very close to the standard CIE coordinate of WLED (0.33, 0.33). Fig. S13(c) shows the photographs of the UV-pumped WLED (Inset) and the operating WLED. Bright white light can be observed when the injection current is 80 mA and the CIE coordinate, CCT and the CRI of the WLED is (0.32, 0.33), 6109 K, and 85, indicating that the WLED is suitable for lighting and displaying. The EL spectra of the WLEDs under different currents from 10 mA to 110 mA are shown in Fig. 6(a). From the EL spectra, the emission intensity of the WLED increases when the driven current increased from 10 to 110 mA and the CIE coordinate, CCT and luminous efficiency shows slight changes from (0.31, 0.32) to (0.32, 0.33), 6085 K to 6116 K and 46.1 lm/W to 47.33 lm/W with the increase of driven current from 10 mA to 110 mA as shown in Fig. 6(b) and Fig. S15. The reason for the color coordinate and CCT show slight changes with injection current is that most the photons emitted from the UV chip can be absorbed by the multi-ZnO-cores@uni-BaSO₄-shell phosphors to convert to visible emission when the injection current is small, while with the increase of the current, some of the emitted photons cannot be absorbed by the multi-ZnO-cores@uni-BaSO₄-shell phosphors, thus portion of the UV emission increases in the whole emission spectrum of the LEDs, leading to the shift of the CCT and color coordinate. These results show that the mZnO@uBaSO₄ phosphors have high stability against the increase of driven current. The images of the WLED under driven current ranging from 10 mA to 110 mA are shown in Fig. 6(c). Obvious white emissions can be observed when the drive current is 10 mA, and the intensity increases gradually with the driven current. In order to assess the color rendering ability of the WLED further, the photographs of some fruits were taken under the lighting of the sunlight and WLED as shown in Fig. 6(d) and (e). It can be clearly seen that the WLED is able to show the true colors of the

fruits. Considering the abundant and bio-compatible substances used in the mZnO@uBaSO₄ phosphors, the results may promise their bright prospect in eco-friendly and healthy lighting and displaying.

3. Conclusions

In conclusion, mZnO@uBaSO₄ phosphors have been prepared via a non-equilibrium sorption process. The mZnO@uBaSO₄ nanocomposite shows improved photo-, thermal- and ambient-stability compare with bare ZnO QDs due to the protection of BaSO₄ shells. The mZnO@uBaSO₄ nanocomposite powders have been packaged onto a UV chip as luminescent phosphors of LEDs, and the CCT, CIE, luminous efficiency and CRI of the LEDs are 6109 K, (0.32, 0.33), 47.33 lm/W and 85, which is close to the standard values of warm white emission. The results reported are suitable for lighting and displaying. It provides a promising pathway towards low cost, eco-friendly, and highly efficient UV-pumped WLEDs.

4. Materials and methods

4.1. Materials

The precursors used in this study include zinc acetate dihydrate ($Zn(Ac)_2 \cdot 2H_2O$, purity > 99%), potassium hydroxide (KOH, purity > 99%), 3-aminopropyltriethoxysilane (APTES, purity > 98%), barium chloride ($BaCl_2 \cdot 2H_2O$, purity > 99.5%), sodium sulfate (Na_2SO_4 , purity > 99%) and ethanol (purity > 99.9%), etc. All of the chemicals were purchased from Macklin Chemistry Co. Ltd (Shanghai, China). Note that all the chemicals used in this work were analytical grade without further purification.

4.2. Synthesis of ZnO QDs

The ZnO QDs were prepared according to the method reported in our previous work [27]. 11 g (50 mmol) $Zn(Ac)_2 \cdot 2H_2O$ was dissolved in 300 ml ethanol solution and the solution was refluxed under continuous stirring for 5 min at room temperature. Then 40 ml 70 mmol KOH solution was added into the $Zn(Ac)_2 \cdot 2H_2O$ ethanol solution under continuous stirring for 5 min, then the solution became colorless and transparent, indicating the ZnO QDs have been formed. Then mixtures of 3 ml deionized water and 800 μl 3-aminopropyltriethoxysilane (APTES) were added into the above solution under continuous stirring for 1 h. After that, the obtained precipitates were washed using ethanol for several times to remove the unreacted precursors. Finally, the ZnO QDs precipitates were dried in an oven at 60 °C for 12 h to form ZnO QD powders.

4.3. Preparation of mZnO@uBaSO₄ phosphors

3 g ZnO QDs powders were dissolved into 100 ml water to prepare ZnO QDs aqueous solution, then 100 ml of 0.5 mol l⁻¹ Na_2SO_4 aqueous solution was added into the ZnO QDs aqueous solution, and the mixture was stirred for 3 min under continuous stirring. Then 100 ml of 0.5 mol l⁻¹ of $BaCl_2$ aqueous solution was added into the mixture resulting in the formation of milky precipitate, indicating the mZnO@uBaSO₄ have been formed. The precipitates were washed using water for several times to remove the unreacted precursors. Finally, the precipitates consisted of mZnO@uBaSO₄ nanocomposite was dried in an oven at 60 °C for 12 h to form mZnO@uBaSO₄ powders.

4.4. Preparation of ZnO@SiO₂ phosphors

10 ml of an ethanol solution containing 0.3 g ZnO QDs and 1 ml of tetraethoxysilane (TEOS) were added to above solution, and then the solution was treated with ultrasound for 30 min. Subsequently, 0.5 ml of ammonia was added slowly to the above solution with continuous stirring for 2 h under a nitrogen atmosphere. After that, the obtained precipitations were washed using ethanol for several times to remove the unreacted precursors. Finally, the ZnO@SiO₂ precipitations were dried in an oven at 60 °C for 10 h.

4.5. Fabrication of LEDs

For the fabrication of WLED, polydimethylsiloxane (PDMS) were premixed with the mZnO@uBaSO₄ phosphors and blue commercial BaMgAl₁₀O₁₇: Eu phosphors with different mass ratios of 2:0.5, 2:0.45, 2:0.4, 2:0.35, 2:0.3, 2:0.25, 2:0.2, 2:0.15 and 2:0.1 (marked as A-I), respectively. The mixed phosphors were packaged onto the UV chip with 365 nm. After that, the as-prepared LEDs were placed into an oven at 100 °C for 1 h to fabricate mZnO@uBaSO₄ based WLEDs.

4.6. Characterizations

X-ray diffraction (XRD) patterns were obtained on X'Pert Pro diffractometer SEM (JSM-6700F) and TEM (JEM-2010) was employed to characterize the size and crystallinity of the samples. EDS were conducted on Oxford Instruments. Fluorescence spectra and PLQYs were obtained on Hitachi F-7000 spectrophotometer. The luminous efficiency is recorded by radiometers PM6612L. UV-vis absorption spectra were obtained using a UH4150 spectrophotometer.

Notes

The authors declare no competing financial interest.

Acknowledgments

This work was supported by the National Natural Science Foundation of China (Grant Nos. 21601159, 61604132, 61505033, 11374296), the National Science Fund for Distinguished Young Scholars (Grant Nos. 61425021).

Appendix A. Supplementary material

Supplementary data associated with this article can be found, in the online version, at <https://doi.org/10.1016/j.jcis.2018.05.100>.

References

- [1] C. Sun, Y. Zhang, K. Sun, C. Reckmeier, T. Zhang, X. Zhang, J. Zhao, C. Wu, W.W. Yu, A.L. Rogach, Combination of carbon dot and polymer dot phosphors for white light-emitting diodes, *Nanoscale* 7 (2015) 12045–12050.
- [2] X. Li, Y. Wu, S. Zhang, B. Cai, Y. Gu, J. Song, H. Zeng, CsPbX₃ Quantum dots for lighting and displays: room-temperature synthesis, photoluminescence superiorities, underlying origins and white light-emitting diodes, *Adv. Funct. Mater.* 26 (2016) 2435–2445.
- [3] Z. Wang, F. Yuan, X. Li, Y. Li, H. Zhong, L. Fan, S. Yang, 53% Efficient red emissive carbon quantum dots for high color rendering and stable warm white-light-emitting diodes, *Adv. Mater.* 29 (2017) 1702910.
- [4] S. Hu, A. Trinchia, P. Atkin, I. Cole, Tunable photoluminescence across the entire visible spectrum from carbon dots excited by white light, *Angew. Chem. Int. Ed.* 54 (2015) 2970–2974.
- [5] D. Yu, F. Cao, Y. Gao, Y. Xiong, H. Zeng, Room-temperature ion-exchange-mediated self-assembly toward formamidinium perovskite nanoplates with finely tunable, ultrapure green emissions for achieving Rec. 2020 displays, *Adv. Funct. Mater.* 28 (2018) 1800248.
- [6] X. Li, Y. Liu, X. Song, H. Wang, H. Gu, H. Zeng, Intercrossed carbon nanorings with pure surface states as low-cost and environment-friendly phosphors for white-light-emitting diodes, *Angew. Chem. Int. Ed.* 54 (2015) 1759–1764.
- [7] M. Sun, S. Qu, Z. Hao, W. Ji, P. Jing, H. Zhang, L. Zhang, J. Zhao, D. Shen, Towards efficient solid-state photoluminescence based on carbon-nanodots and starch composites, *Nanoscale* 6 (2014) 13076–13081.
- [8] Y. Zhai, D. Zhou, P. Jing, D. Li, H. Zeng, S. Qu, Preparation and application of carbon-nanodot@NaCl composite phosphors with strong green emission, *J. Colloid Interface Sci.* 497 (2017) 165–171.
- [9] J. He, Y. He, Y. Chen, B. Lei, J. Zhuang, Y. Xiao, Y. Liang, M. Zheng, H. Zhang, Y. Liu, Solid-state carbon dots with red fluorescence and efficient construction of dual-fluorescence morphologies, *Small* 13 (2017) 1700075.
- [10] Y. Fan, X. Guo, Y. Zhang, Y. Lv, J. Zhao, X. Liu, Efficient and stable red emissive carbon nanoparticles with a hollow sphere structure for white light-emitting diodes, *ACS Appl. Mater. Int.* 8 (2016) 31863–31870.
- [11] X. Zhuang, H. Zhang, K. Ye, Y. Liu, Y. Wang, Two host-dopant emitting systems realizing four-color emission: a simple and effective strategy for highly efficient warm-white organic light-emitting diodes with high color-rendering index at high luminance, *ACS Appl. Mater. Int.* 8 (2016) 11221–11225.
- [12] M. Peng, X. Yin, P.A. Tanner, M.G. Brik, P. Li, Site occupancy preference, enhancement mechanism, and thermal resistance of Mn⁴⁺ red luminescence in Sr₄Al₁₄O₂₅: Mn⁴⁺ for warm WLEDs, *Chem. Mater.* 27 (2015) 2938–2945.
- [13] W. Lv, Y. Jia, Q. Zhao, M. Jiao, B. Shao, W. Lü, H. You, Crystal structure and luminescence properties of Ca₈Mg₃Al₂Si₇O₂₈: Eu²⁺ for WLEDs, *Adv. Opt. Mater.* 2 (2014) 183–188.
- [14] E. Matioli, S. Brinkley, K.M. Kelchner, Y. Hu, S. Nakamura, S. DenBaars, J. Speck, C. Weisbuch, High-brightness polarized light-emitting diodes, *Light: Sci. Appl.* 1 (2012) e22.
- [15] D. Chen, W. Xiang, X. Liang, J. Zhong, H. Yu, M. Ding, H. Lu, Z. Ji, Advances in transparent glass-ceramic phosphors for white light-emitting diodes—a review, *J. Eur. Ceram. Soc.* 35 (2015) 859–869.
- [16] H.S. Jang, Y.H. Won, D.Y. Jeon, Improvement of electroluminescent property of blue LED coated with highly luminescent yellow-emitting phosphors, *Appl. Phys. B* 95 (2009) 715–720.
- [17] Z. Wu, J. Liu, M. Gong, Thermally stable luminescence of SrMg₂(PO₄)₂: Eu²⁺ phosphor for white light NUV light-emitting diodes, *Chem. Phys. Lett.* 466 (2008) 88–90.
- [18] Q. Yu, Y. Liu, S. Wu, X. Lü, X. Huang, X. Li, Luminescent properties of Ca₂SiO₄: Eu³⁺ red phosphor for trichromatic white light emitting diodes, *J. Rare Earth.* 26 (2008) 783–786.
- [19] P. Dai, C. Li, X. Zhang, J. Xu, X. Chen, X. Wang, Y. Jia, X. Wang, Y. Liu, A single Eu²⁺-activated high-color-rendering oxychloride white-light phosphor for white-light-emitting diodes, *Light: Sci. Appl.* 5 (2006) e16024.
- [20] M.M. Haque, H. Lee, D. Kim, Luminescent properties of Eu³⁺-activated molybdate-based novel red-emitting phosphors for LEDs, *J. Alloy. Compd.* 481 (2009) 792–796.
- [21] Q. Zhang, C. Wang, L. Ling, S. Chen, Fluorescent nanomaterial-derived white light-emitting diodes: what's going on, *J. Mater. Chem. C* 2 (2014) 4358–4373.
- [22] N. Chen, Y. He, G. Du, Preparation and luminescence of europium-doped lanthanum fluoride-benzoic acid hybrid nanostructures, *Mater. Sci. Semicon. Proc.* 24 (2014) 62–67.
- [23] V.R. Bandi, B.K. Grandhe, H. Woo, K. Jang, D. Shin, S. Yi, J. Jeong, Luminescence and energy transfer of Eu³⁺ or/and Dy³⁺ co-doped in Sr₃AlO₄F phosphors with NUV excitation for WLEDs, *J. Alloys Compd.* 538 (2012) 85–90.
- [24] L. Wang, R. Xie, Y. Li, X. Wang, C. Ma, D. Luo, T. Takeda, Y. Tsai, R. Liu, N. Hiroasaki, Ca_{1-x}Li_xAl_{1-x}Si_{1+x}N₃: Eu²⁺ solid solutions as broadband, color-tunable and thermally robust red phosphors for superior color rendition white light-emitting diodes, *Light: Sci. Appl.* 5 (2016) e16155.
- [25] X. Li, J.D. Budai, F. Liu, J.Y. Howe, J. Zhang, X. Wang, Z. Gu, C. Sun, R.S. Meltzer, Z. Pan, New yellow Ba_{0.93}Eu_{0.07}Al₂O₄ phosphor for warm-white light-emitting diodes through single-emitting-center conversion, *Light: Sci. Appl.* 2 (2013) e50.
- [26] H. Duan, Y. Jiang, Y. Zhang, D. Sun, C. Liu, J. Huang, X. Lan, H. Zhou, L. Chen, H. Zhong, High quantum-yield CdSe_xS_{1-x}ZnS core/shell quantum dots for warm white light-emitting diodes with good color rendering, *Nanotechnology* 24 (2013) 285201.
- [27] K. Liu, C. Shan, R. Zhou, Q. Zhao, D. Shen, Large-scale synthesis of ZnO nanoparticles and their application as phosphors in light-emitting devices, *Opt. Mater. Express* 7 (2017) 2682.
- [28] E. Jang, S. Jun, H. Jang, J. Lim, B. Kim, Y. Kim, White-light-emitting diodes with quantum dot color converters for display backlights, *Adv. Mater.* 22 (2010) 3076–3080.
- [29] H. Zeng, G. Duan, Y. Li, S. Yang, X. Xu, W. Cai, Blue luminescence of ZnO nanoparticles based on non-equilibrium processes: defect origins and emission controls, *Adv. Funct. Mater.* 20 (2010) 561–572.
- [30] K. Liu, C. Shan, G. He, R. Wang, L. Dong, D. Shen, Rewritable painting realized from ambient-sensitive fluorescence of ZnO nanoparticles, *Sci. Rep.* 7 (2017) 42232.
- [31] R. Zhou, Q. Zhao, K. Liu, Y. Lu, L. Dong, C. Shan, Europium-decorated ZnO quantum dots as a fluorescent sensor for the detection of an anthrax biomarker, *J. Mater. Chem. C* 5 (2017) 1685–1691.
- [32] H. Xiong, ZnO nanoparticles applied to bioimaging and drug delivery, *Adv. Mater.* 25 (2013) 5329–5335.
- [33] Y. Liu, K. Ai, Q. Yuan, L. Lu, Fluorescence-enhanced gadolinium-doped zinc oxide quantum dots for magnetic resonance and fluorescence imaging, *Biomaterials* 32 (2011) 1185–1192.

- [34] B. Zhao, Y. Yao, K. Yang, P. Rong, P. Huang, K. Sun, X. An, Z. Li, X. Chen, W. Li, Mercaptopropionic acid-capped Mn²⁺: ZnSe/ZnO quantum dots with both downconversion and upconversion emissions for bioimaging applications, *Nanoscale* 6 (2014) 12345–12349.
- [35] S. Afroz, H. Medhi, S. Maity, G. Minhas, S. Battu, J. Giddaluru, K. Kumar, P. Paik, N. Khan, Mesoporous ZnO nanocapsules for the induction of enhanced antigen-specific immunological responses, *Nanoscale* 9 (2017) 14641–14653.
- [36] X. Cai, Y. Luo, W. Zhang, D. Du, Y. Lin, PH-sensitive ZnO quantum dots-doxorubicin nanoparticles for lung cancer targeted drug delivery, *ACS Appl. Mater. Int.* 8 (2016) 22442–22450.
- [37] N. Tripathy, R. Ahmad, H.A. Ko, G. Khang, Y. Hahn, Enhanced anticancer potency using an acid-responsive ZnO-incorporated liposomal drug-delivery system, *Nanoscale* 7 (2015) 4088–4096.
- [38] F. Muhammad, M. Guo, W. Qi, F. Sun, A. Wang, Y. Guo, G. Zhu, PH-triggered controlled drug release from mesoporous silica nanoparticles via intracellular dissolution of ZnO nanolids, *J. Am. Chem. Soc.* 133 (2011) 8778–8781.
- [39] H. Hong, F. Wang, Y. Zhang, S.A. Graves, S.B.Z. Eddine, Y. Yang, C.P. Theuer, R.J. Nickles, X. Wang, W. Cai, Red fluorescent zinc oxide nanoparticle: a novel platform for cancer targeting, *ACS Appl. Mater. Int.* 7 (2015) 3373–3381.
- [40] X. Tang, E.S.G. Choo, L. Li, J. Ding, J. Xue, Synthesis of ZnO nanoparticles with tunable emission colors and their cell labeling applications, *Chem. Mater.* 22 (2010) 3383–3388.
- [41] D. Guo, C. Shan, S. Qu, D. Shen, Highly sensitive ultraviolet photodetectors fabricated from ZnO quantum dots/carbon nanodots hybrid films, *Sci. Rep.* 4 (2014) 7469.
- [42] X. Liu, H. Du, P. Wang, T. Lim, X.W. Sun, A high-performance UV/visible photodetector of Cu₂O/ZnO hybrid nanofilms on SWNT-based flexible conducting substrates, *J. Mater. Chem. C* 2 (2014) 9536–9542.
- [43] J. Park, J. Lee, Y. Noh, K. Shin, D. Lee, Flexible ultraviolet photodetectors with ZnO nanowire networks fabricated by large area controlled roll-to-roll processing, *J. Mater. Chem. C* 4 (2016) 7948–7958.
- [44] D. Gedamu, I. Paulowicz, S. Kaps, O. Lupan, S. Wille, G. Haidarschin, Y.K. Mishra, R. Adelung, Rapid fabrication technique for interpenetrated ZnO nanotrapod networks for fast UV sensors, *Adv. Mater.* 26 (2014) 1541–1550.
- [45] D.I. Son, B.W. Kwon, D.H. Park, W. Seo, Y. Yi, B. Angadi, C. Lee, W.K. Choi, Emissive ZnO – graphene quantum dots for white-light-emitting diodes, *Nat. Nanotechnol.* 7 (2012) 465–471.
- [46] J. Chen, D. Zhao, C. Li, F. Xu, W. Lei, L. Sun, A. Nathan, X.W. Sun, All solution-processed stable white quantum dot light-emitting diodes with hybrid ZnO@TiO₂ as blue emitters, *Sci. Rep.* 4 (2015) 4085.